PERSPECTIVE • OPEN ACCESS

Particle swarm optimization of GaAs-AlGaAS nanowire photonic crystals as two-dimensional diffraction gratings for light trapping

To cite this article: Luca Zagaglia *et al* 2022 *Nano Ex.* **3** 021001

View the article online for updates and enhancements.

NANO EXPRESS

PERSPECTIVE

Particle swarm optimization of GaAs-AlGaAS nanowire photonic crystals as two-dimensional diffraction gratings for light trapping
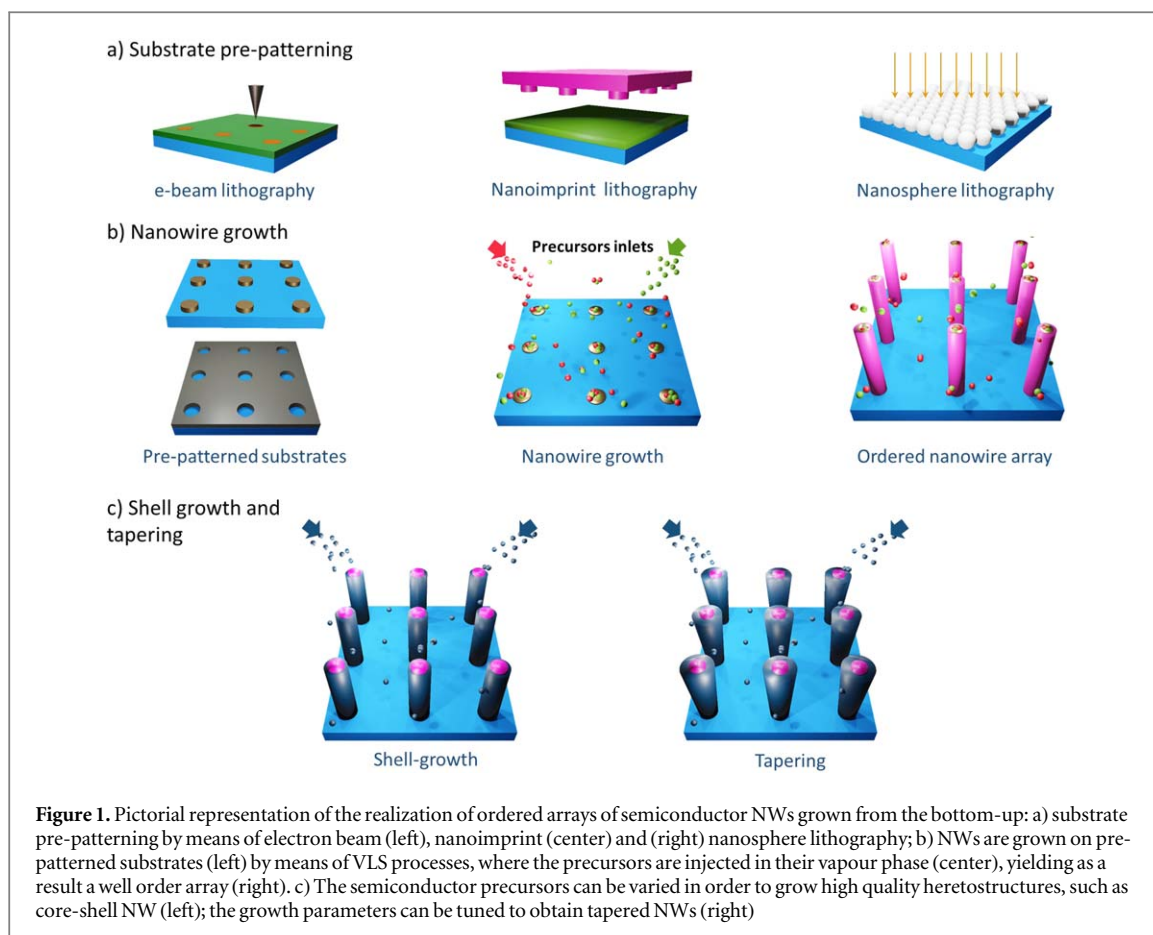
Luca Zagaglia[1,4] , Valeria Demontis[2], Francesco Rossella[3] and Francesco Floris[1,4]

1   Tyndall National Institute, University College Cork, Cork, Ireland
2   NEST Laboratory, Scuola Normale Superiore and Istituto Nanoscienze-CNR, Pisa , Italy
3   Dipartimento di Scienze Fisiche, Informatiche e Matematiche, Università di Modena e Reggio Emilia, via Campi 213/a-41125 Modena, Italy
4   Department of Physics, University of Pavia, Pavia, IT27100, Italy.

E-mail: francesco.rossella@unimore.it

Abstract

Semiconductor nanowire ordered arrays represent a class of bi-dimensional photonic crystals that can be engineered to obtain functional metamaterials. Here is proposed a novel approach, based on a particle swarm optimization algorithm, for using such a photonic crystal concept to design a semiconductor nanowire-based two-dimensional diffraction grating able to guarantee an in-plane coupling for light trapping. The method takes into account the experimental constraints associated to the bottom-up growth of nanowire arrays, by processing as input dataset all relevant geometrical and morphological features of the array, and returns as output the optimised set of parameters according to the desired electromagnetic functionality of the metamaterial. A case of study based on an array of tapered GaAs-AlGaAs core–shell nanowire heterostructures is discussed.

1. Introduction

Photonic crystals (PhC) [1], engineered nanostructured dielectric systems with a periodic spatial modulation of the refractive index, are established as an excellent technological platform for light manipulation and control [2, 3]. In particular, thanks to their high symmetry, are excellent platforms to design diffraction gratings able to guarantee the fine control of light coupling along certain directions for specific frequencies, depending on the design parameters The employment of optimised photonic structures to enhance specific optical functionalities is a vibrant research topic. Such a feature is largely exploited for light trapping based applications [4] such as solar cells [5, 6] and sensing [7–11], or to control the emission of optical emitters [12–14]. In this context, ordered semiconductor nanowire (NW) ensembles grown onto a substrate are a suitable starting platform [15–17]. In this paper, we discuss an innovative protocol based on a particle swarm optimization (PSO) algorithm [18, 19] to tune the periodicity of an ordered array of GaAs-AlGaAs tapered core–shell NWs where Fabry–Perot oscillations sustained by the external shell give the light trapping effect, yielding the NW array to act as a diffraction grating. The PSO represents a powerful and versatile tool for the optimization of complex photonic structures as its simple and intuitive mathematical structure results in a reasonably fast development, debugging and easy implementation inside the used electromagnetic simulation framework. This is a crucial advantage compared to other class of evolutionary algorithm, as for instance genetic algorithms. In this work the PSO is tailored resulting in a valuable routine to optimize the relative reflectance by directly tailoring the optical response of an ordered ensemble of core–shell NW array, leading the way to a systematic optimization and further engineering of platforms based on these type of structure for real applications. Our choice of the specific case of study stands on three pillars: (i) the emerging interest of metasurface-based optical sensors exploiting direct and immediate measurement methods; (ii) GaAs/AlGaAs core–shell NW having been proven to display both computationally and experimentally far field reflectance spectra with features compatible with a Fabry-Perrot resonator; (iii) these features being of potential interest to reveal changes in the surrounding

Figure 1. Pictorial representation of the realization of ordered arrays of semiconductor NWs grown from the bottom-up: a) substrate pre-patterning by means of electron beam (left), nanoimprint (center) and (right) nanosphere lithography; b) NWs are grown on pre-patterned substrates (left) by means of VLS processes, where the precursors are injected in their vapour phase (center), yielding as a result a well order array (right). c) The semiconductor precursors can be varied in order to grow high quality heretostructures, such as core-shell NW (left); the growth parameters can be tuned to obtain tapered NWs (right)

environment - variation of the background refractive index - exploitable as a potential signal for future development of sensors. The experimental constraints associated to the bottom-up growth of III-V semiconductor NW arrays are briefly discussed, and are taken into account in the calculation by processing as input dataset all relevant geometrical/morphological features of the array.

2. Realization of bottom-up nanowire arrays: a brief overview

Ordered arrays of semiconductor NWs can efficiently be realized exploiting the bottom-up paradigm and relying on two main techniques: nanoparticle-assisted growth, which is at present the most commonly used technique [20, 21], and catalyst–free growth [22], often combined with selective area epitaxy [23]. In both these approaches, different nanolithography methods are employed to define on the growth substrate a pattern of seeds, which do assist the growth of NWs at specified locations [24]. This pattern consists in an array of metal nanoparticles [25], or in a pattern of holes inside a thin amorphous oxide layer deposited on the substrate [26]. These techniques allow to reach a very fine control over the size, shape and material composition of each individual NW in the array. The left and center panels in figure 1(a) show two of the most used surface nanopatterning techniques, i.e. electron beam and nanoimprint lithography, as well as an example of an alternative cheaper option i.e. nanosphere lithography (right panel). The NW growth on the pre-patterned substrates (figures 1(b)–(1)) is mainly obtained by vapor–liquid–solid (VLS) processes [21], by injecting the semiconductor source materials in their vapor phase in a reactor chamber and finely controlling the growth parameters, such as precursor's flows, temperature, pressure, etc (figure 1(b)). As shown in figure 1(c) (left panel), the materials precursors injected into the growth chamber can opportunely be varied in order to obtain high quality heterostructures, e.g. in the radial direction (core-multishell heterostructures), with atomically sharp interfaces [27–29]. The control of the growth parameters also allows the variation of the NW diameter along the axis (figure 1(c)-right), which results in NWs with inclined sidewalls (tapering) [30].

3. Array design using particle swarm optimization algorithms

Resorting on the different methods briefly discussed in the previous section, virtually infinite types of NW arrays can be engineered. The NW material and the geometrical parameters of the array fix its electromagnetic response, and the
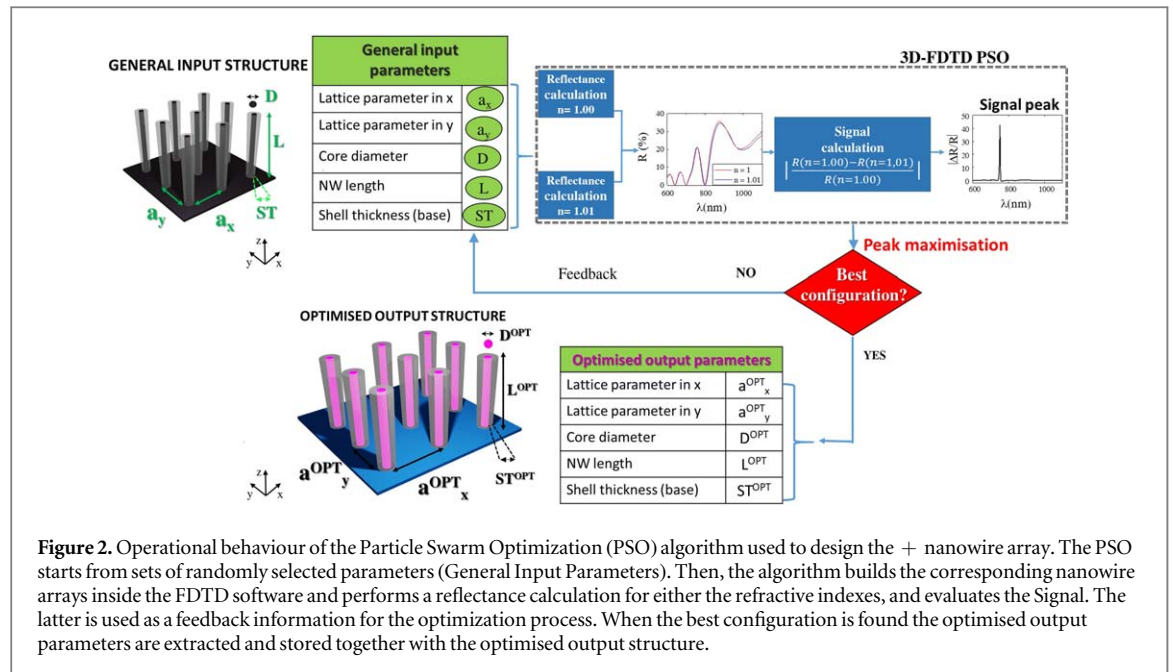
Figure 2. Operational behaviour of the Particle Swarm Optimization (PSO) algorithm used to design the + nanowire array. The PSO starts from sets of randomly selected parameters (General Input Parameters). Then, the algorithm builds the corresponding nanowire arrays inside the FDTD software and performs a reflectance calculation for either the refractive indexes, and evaluates the Signal. The latter is used as a feedback information for the optimization process. When the best configuration is found the optimised output parameters are extracted and stored together with the optimised output structure.

array can be conceived as a metamaterial. To optimize the entire set of array parameters toward a specific optical response or functionality, a significant benefit can come from the use of PSO algorithm, a heuristic population-based search method [19, 20]. Here, an initial randomly generated population (swarm) performs an iterative process seeking for an optimal design solution in terms of a specific fitness function. As a case of study to illustrate this approach we address the problem of the far field reflectance in arrays of GaAs-AlGaAs core–shell NWs, with the goal to achieve optical sensing functionalities based on the occurrence of sharp peaks in the relative reflectance variation ($\Delta R/R$) of the array, as previously reported for disordered ensembles of homogeneous III-V NWs [31]. Figure 2 shows the operational behaviour of the algorithm applied to the chosen NW array. The general input structure is composed by a square lattice of GaAs-AlGaAs core–shell NWs. Notably, this system was previously identified as displaying an intriguing electromagnetic behaviour [32] with great potential for sensing [17]. The input structures are considered with their geometrical features characterized by five general parameters namely the lattice parameter in x (a_x) and y (a_y), core diameter (D), NW length (L) and shell thickness the NW base (ST). The latter are selected in order to define and control either the geometry of the entire ensemble as well as of the single NW, in accordance with the experimental constraints related to the growth process. The initial values of the five parameters are included in a numerical array, used to initialize the general structures, and as input of a customized Particle Swarm Optimization (PSO) Algorithm [19, 20]. The PSO is implemented inside the commercial Finite Difference Time Domain (FDTD) software Lumerical FDTD [33], in order to be automatically controlled by: (i) choosing the general parameters in appropriate subsets complying with the fabrication constrains imposed by the growth processes, (ii) building the corresponding structure, (iii) setting-up the entire full three dimensional (3D) FDTD simulation, (iv) running the simulation and collecting the results, (v) managing the analysis process. The goal of this study being to computationally address NWs arrays structure with enhanced sensing functionalities, we aim at identifying structures able to detect very small variations in the background refractive index (e.g. due to the presence of analytes or chemical species in the environment). The phenomenon enabling the sensor operation being the variation in the reflectivity spectra, we calculated two reflectivity spectra using a background refractive index of 1.00 (array in air) and 1.01 (array in environment with refractive index perturbed of 1% respect to air). To measure the variations induced in our system reflectance by this small perturbation, we calculated the differential reflectance, which is the signal enabling the optical transduction in the proposed sensor. In this framework, the relative reflectance represents the fitness function in our PSO, which directly optimize the potential signal of a sensor in the desired wavelength range by changing the structural parameters of the NW array. The core concept of the entire optimization procedure is thus based on the calculation of the signal $\Delta R/R$ for each structure according to [17]:

$$\frac{\Delta R}{R} = \left| \frac{R(n = 1.00) - R(n = 1.01)}{R(n = 1.00)} \right|$$

where $\Delta R/R$ is the relative reflectance variation, R (n = 1.00) is the reference R calculated considering the array immersed in air, and R(n = 1.01) is the R spectrum calculated considering the array immersed in an environment having a refractive index of 1.01. For the proposed sensing scheme, the crucial point is the introduction, by the analytes, of a shift-as large as possible - in the reflectance valleys or peaks, highlighted

through the point-by-point ratio of the two spectra (reference and analyte), or equivalently the ΔR/R function. This will correspond to the highest possible signal-to-noise ratio, while the ΔR/R ratio represents the fitness function in the PSO design routine. In principle, the complexity of the fitness function can be increased on demand: multiple parameters can be optimized and controlled using the PSO, which may find the best trade off in terms of ΔR/R intensity and wavelength position of any ΔR/R spike(s). Operatively, the PSO creates each FDTD simulation by setting periodic Bloch boundary conditions in the x-y plane, and Perfect Matched Layer along the z-direction to calculate the *R* spectrum of the entire array, by simulating an opportune limited 3D-FDTD cell, i.e., the unit cell of the array, with a x and a y span equal to a_x and a_y, respectively. The NWs are built on a GaAs substrate with a GaAs core and a $Al_xGa_{1-x}As$ tapered-shell, with x = 0.1. The optical properties of the materials are defined through the built-in material database. A s-polarized plane-wave source at normal incidence, with the electric field oscillating along the **y** direction, is used to excite the Bloch-states from the top collecting the *R* spectrum through a power monitor placed behind the light source in the spectral interval (600 ÷ 900) nm. Our structure being symmetric with respect to rotations upon the *z* axis (according to figure 2), and the analysis being conducted at normal incidence, we do not expect differences in the optical response to a s- or p-polarized plane-wave source: the two polarization states are degenerate, the metasurface does not distinguish or separate them.

An Alienware Area 51 (Dell) with a liquid-cooled Intel® Core™ processor i9-7960X (16 core, 32 threads) and 64GB of RAM is used to perform the simulation, and it took approximately 24 h to complete an entire optimization process. Furthermore, a customized mesh with a 5 nm resolution created through a proper mesh override around the NW region was found adequate after performing appropriate convergence tests.

Thus, the PSO operates the signal calculation and then the algorithm extracts the intensity related to the signal peak, exploited as a feedback for scanning the parameter space aiming at the peak optimization. Eventually, the PSO converges and the numeric array with the optimised output parameters can be extracted and the signal peak computed and stored. Then, the electromagnetic (EM) field expansion related to the optimized structure is computed to look at the EM features of the localized modes. The case of study discussed in our work highlights how the PSO can be applied to optimize dielectric metasurfaces. In future works combining experiments and simulation, the optical dispersion of each material involved should be performed and then imported inside the library to have the better adhesion possible to the experimental outcomes. Overall, we consider that is worth performing this type of analysis exploiting the experimental optical dispersions of the materials and then addressing the neff resorting to computational methods

4. Optimized array: light diffraction and trapping, photonic bands

Figure 3 synthesizes the outcome of the PSO process, showing two optimised structures, characterised by the EM field expansion focused at the top or at the bottom of the NWs. Panel (a), summarizes the optimized five parameters with the corresponding signal peak tuned at $\lambda^{OPT1} = 707$nm. Here the mode is mainly TM-polarized, i.e. the electric field oscillates along the **z**-direction, leading to a potential EM field confinement due to the excitation of a spatially confined mode, and enabling for a dipolar expansion shape with an emission in the **x-y** plane resulting in a suppression of *R* at the aforementioned wavelength.

To verify the confinement, the EM field expansion was performed and figure 3, panels (b) and (c), shows a cross-section along the **y-z** plane of the E_z scalar component.

The tapering of the shell induces an in-plane light scattering that enables a rotation of the polarization state, leading to the excitation of a TM-polarized spatially confined mode resulting in a minimum of the *R* spectrum. The E_z field shows an ordered arrangement of maxima and minima localized at the interfaces between the different materials, in accordance with [17]. In particular, E_z reaches the highest value at the top corner of the shell-air interface for z = 1200nm, where a x-y cross section displays a circular shape consistent with a dipolar field distribution.

To further understand the behaviour of the spatially confined E_z scalar component sustained by the NWs, we investigate [34] the frequency dispersion curve $f(\mathbf{k})$, where *f* indicates the frequency and **k** the wave vector. The f(**k**) curves for the optimized structure 1 is reported in figure 3 panel (d). Here, the yellow lines represent the modes at a defined (*f*, **k**) point. As can be seen, the λ^{OPT1}, i.e. 424THz, falls in the region where the EM field confinement is permitted.

Figure 3 panel (e) shows the best parameters of the PSO optimized structure 2 together with the optimized signal with a peak at $\lambda^{OPT2} = 829$ nm. Again, the corresponding EM field expansion shows its link with a spatially confined E_z scalar component, as can be seen from its real part, figure 3 panels (f) and (g). Here, the field is confined in the shell region with an ordered pattern of maxima and minima, consequence of the coherent cross-talk across the periodic array, with the same dipolar features seen previously. However, E_z is pushed towards the base of the NW with the field partially expanding in the outer region. In this case, from figure 3 panel (h), it can be noticed that λ^{OPT2}, i.e. 362THz, falls at the band edge of the region where there is an overlap
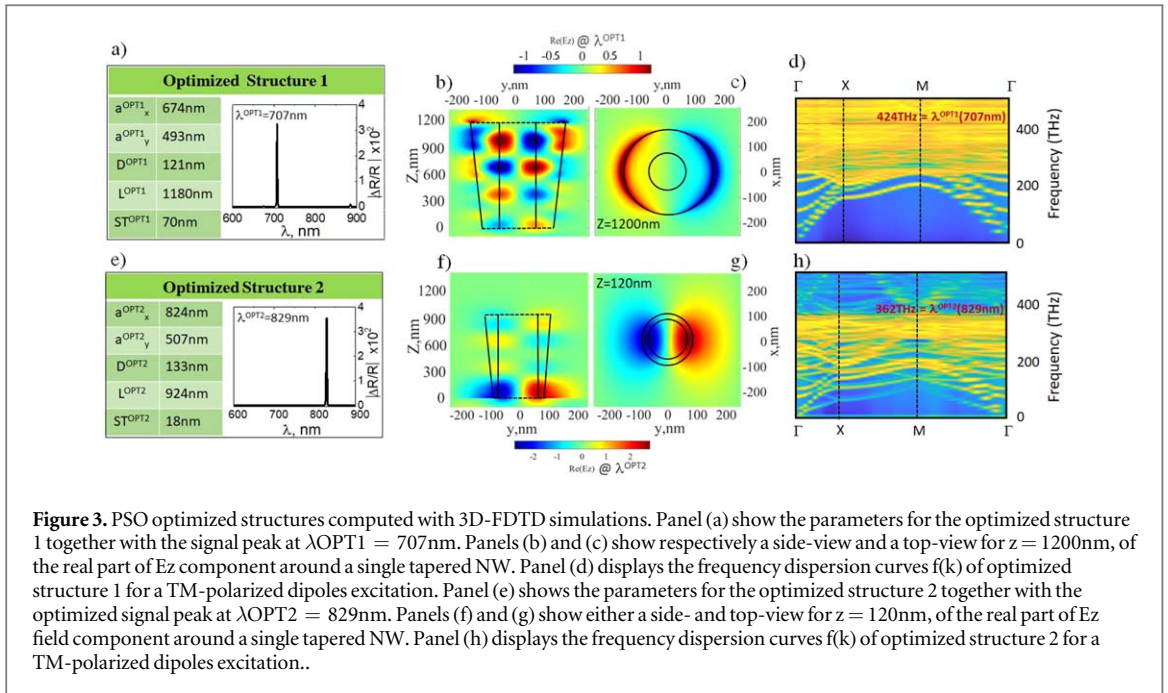
Figure 3. PSO optimized structures computed with 3D-FDTD simulations. Panel (a) show the parameters for the optimized structure 1 together with the signal peak at $\lambda OPT1 = 707$nm. Panels (b) and (c) show respectively a side-view and a top-view for $z = 1200$nm, of the real part of Ez component around a single tapered NW. Panel (d) displays the frequency dispersion curves f(k) of optimized structure 1 for a TM-polarized dipoles excitation. Panel (e) shows the parameters for the optimized structure 2 together with the optimized signal peak at $\lambda OPT2 = 829$nm. Panels (f) and (g) show either a side- and top-view for $z = 120$nm, of the real part of Ez field component around a single tapered NW. Panel (h) displays the frequency dispersion curves f(k) of optimized structure 2 for a TM-polarized dipoles excitation..

between $f(\mathbf{k})$ curves, resulting to be in accordance with the mode field expansion. The dispersion curves of the two optimized structures are different due to the diverse geometrical features. In fact, by varying the structural parameters, i.e. a_x, a_y, D, L, and ST, it is possible to change the fraction of total area of the unit cell occupied by high refractive index materials, here GaAs and AlGaAs, with respect to the low refractive index, i.e. air, thus controlling the effective refractive index of the periodic metasurface. In particular, optimized structure 1 shows a higher fraction of high index materials resulting in a band of accessible states at higher frequencies with respect to optimized structure 2. Therefore, this results in the possibility of tuning the signal peak, by varying the structural parameters, across the $(700 \div 850)$ nm wavelength interval. The discussed wavelengths fall inside the VIS-NIR range, a region of increasing interest particularly for bio-sensing applications: the easy availability of off-the-shelf light source in this range makes it promising to target future mass-production of photonic biosensors. In addition, the two wavelengths are compatible with the absorption peaks of organic fluorophores employed with plasmonic metasurfaces, offering the possibility to compare the sensing performances of the latter with the all-dielectric NW array under study. The analysis of the dispersion curves reveals the ability of the algorithm to drive the metasurface to display optical conduction or, equivalently, the availability of photonic states, in the targeted wavelength range suitable for sensing purposes: the desired reflectance response leads to high sensitivity in the variation of the background refractive index, and therefore to enhanced signal in the relative reflectance.

5. Conclusions

A customized PSO algorithm was exploited to perform the optimization of the relative reflectance variation $\Delta R/R$ of a bi-dimensional GaAs core-Al$_x$Ga$_{1-x}$As tapered shell NW ordered array exploiting fully 3D-FDTD simulations. This approach enabled us to study the capability of the structure to potentially confine an impinging EM field into a localized in-plane mainly z-polarized confined modes. Two optimized structures were reported with intensities of the optimized signal peaks of the order of 10^2 for both structures, tuned at $\lambda^{OPT1} = 707$nm and $\lambda^{OPT2} = 829$nm, respectively.

Through an EM field expansion analysis, the peaks were demonstrated to be associated with an ordered arrangement of maxima and minima localized at the interfaces between the different materials for optimized structure 1, and a dipolar distribution at the bottom shell-substrate interface for optimized structure 2. Here, the EM field pattern was shown to be ordered and supported by the coherency enabled by the fine tuning of the periodicity of the array. Finally, the response of the arrays to a TM-polarized dipolar field was studied through a dispersion curves $f(\mathbf{k})$ analysis, showing the existence of several accessible states for EM field confinement available at λ^{OPT1} and λ^{OPT2}.

Data availability statement

The data that support the findings of this study are available upon reasonable request from the authors.

ORCID iDs

Luca Zagaglia ⬤ https://orcid.org/0000-0002-4402-3031
Francesco Rossella ⬤ https://orcid.org/0000-0002-0601-4927
Francesco Floris ⬤ https://orcid.org/0000-0003-1576-6212

References

[1] Yablonovitch E 1987 *Phys. Rev. Lett.* **58** 2059–62
[2] Lemoult F, Kaina N, Fink M and Lerosey J 2013 *Nature Physics* **9** 55–60
[3] Joannopoulos J D, Johnson S G, Winn J N and Meade R D 1995 *Photonic Crystals: Molding the Flow of Light*
[4] Muskens O L, Diedenhofen S L, Kaas B C, Algra R E, Bakkers E P, Rivas J G and Lagendijk A 2009 *Nano Lett.* **9** 930–4
[5] Muskens O L, Rivas J G, Algra R E, Bakkers E P and Lagendijk A 2008 *Nano Lett.* **8** 2638–2642
[6] Goktas N I, Wilson P, Ghukasyan D, Wagner D, McNamee S and LaPierre R R 2018 *Appl. Phys. Rev.* **5** 041305
[7] Floris F *et al J. Phys. Chem. Lett.* 2014 **5** 2935–40
[8] Garnett E and Yang P 2010 *Nano Lett.* **10** 1082–7
[9] Bhaskar S, Kumar Singh A, Das P, Jana P, Kanvah S, Bhaktha S and Sathish Ramamurthy S 2020 *ACS Appl. Mater. Interfaces* **12** 34323–34336
[10] Bhaskar S, Das P, Srinivasan V, Kanvah S, Bhaktha S and Sathish Ramamurthy S 2020 *J. Phys. Chem. C* **124** 7341–52
[11] Bhaskar S, Das P, Srinivasan V, Bhaktha S and Sathish Ramamurthy 2022 *Mater. Res. Bull.* **145** 111558
[12] Fornasari L, Floris F, Patrini M, Canazza G, Guizzetti G, Comoretto D and Marabelli F 2014 *Appl. Phys. Lett.* **105** 053303
[13] Fornasari L, Floris F, Patrini M, Comoretto D and Marabelli F 2016 *Phys. Chem. Chem. Phys.* **18** 14086–93
[14] Bhaskar S, Das P, Moronshing M, Rai A, Subramaniam C, Bhaktha S and Sathish Ramamurthy S 2021 *Nanophotonics* **13** 3417–31
[15] LaPierre R R, Robson M, Azizur-Rahman K M and Kuyanov P J 2017 *Phys. D Appl. Phys.* **50** 123001
[16] Zagaglia L, Demontis V, Rossella F and Floris F 2021 *Nanotechnology* **32** 335502
[17] Demontis V, Marini A, Floris F, Sorba L and Rossella F 2020 *AIP Conference Proceedings* **2257** 020009
[18] Zagaglia L, Floris F and O'Brien P A J 2021 *Lightwave Technol.* **39** 5028–34
[19] Zagaglia L, Floris F and O'Brien P 2019 *PhotonIcs & Electromagnetics Research Symp. - Spring (PIERS-Spring)* pp 234–41
[20] Wagner R S and Ellis W C 1964 *Applied physics letters* **4** 89–90
[21] Dasgupta N P, Sun J, Liu C, Brittman S, Andrews S C, Lim J, Gao H, Yan R and Yang P 2014 *Adv. Mater.* **6** 2137–84
[22] Güniat L, Caroff P, Fontcuberta I and Morral A 2019 *Chem. Rev.* **119** 8958–71
[23] Bauer B, Rudolph A, Soda M, Fontcuberta I, Morral A, Zweck J, Schuh D and Reiger E 2010 *Nanotechnology* **21** 435601
[24] Demontis V, Zannier V, Sorba L and Rossella F 2021 *Nanomaterials* **11** 2079
[25] Mårtensson T, Borgstrom M, Seifert W, Ohlsson B J and Samuelson L 2003 *Nanotechnology* **14** 1255–8
[26] Mandl B, Stangl J, Hilner E, Zakharov A A, Hillerich K, Dey A W, Samuelson L, Bauer G, Deppert K and Mikkelsen A 2010 *Nano Lett.* **10** 4443–9
[27] Battiato S *et al* 2019 *Nanotechnology* **30** 194004
[28] Arif O, Zannier V, Li A, Rossi F, Ercolani D, Beltram F and Sorba L 2020 *Crystal Growth & Design* **20** 1088–96
[29] Salimian S, Arif O, Zannier V, Ercolani D, Rossi F, Momtaz Z S, Beltram F, Roddaro S, Rossella F and Sorba L 2020 *Nano Research* **13** 1065–70
[30] McIntyre P C and Fontcuberta I Morral A 2020 *Mater. Today Nano* **9** 100058
[31] Floris F *et al* 2017 *Nanomaterials* **7** 400
[32] Floris F *et al* 2019 *Materials* **12** 3572
[33] Lumerical Inc. Available online: (http://lumerical.com/tcad-products/fdtd/)
[34] Babaei H A, Serajmohammadi S, Mehdicadeh F and Andalib A 2015 *J. Opt. Commun.* **36** 109–14